Physical Communication 44 (2021) 101234

Contents lists available at ScienceDirect

Physical Communication

journal homepage: www.elsevier.com/locate/phycom

Full length article

Joint 3D placement and multi-beam design for UAV-assisted wireless power transfer networks

Xiangyang Duan [a], Shaopeng Ao [b], Wanmei Feng [b], Jie Tang [b,1], Juncheng Hu [c,*]

[a] ZTE Corporation, Shenzhen, China
[b] School of Electronic and Information Engineering, South China University of Technology, Guangzhou, China
[c] Guilin Medical University, Guilin, China

ARTICLE INFO

Article history:
Received 31 July 2020
Received in revised form 24 September 2020
Accepted 30 October 2020
Available online 30 November 2020

Keywords:
Butler matrix
Multi-beam
UAV 3D placement
Wireless power transfer

ABSTRACT

This paper investigates an unmanned aerial vehicle (UAV)-enabled wireless power transfer (WPT) system, where a UAV acts as the energy transmitter (ET) to deliver radio frequency (RF) energy to a set of energy receivers (ERs). Our aim is to maximize the total harvested energy at all ERs by jointly optimizing the three-dimensional (3D) position of the UAV and beam pattern. However, the optimization problem which takes into account the coverage radius of the UAV and beam scanning range, is formulated as a non-convex problem and hence is difficult to solve. To address this problem, we propose a low-complexity iterative algorithm that decomposes the original problem into three sub-problems and solves the 2D position of the UAV, flight altitude and beam pattern in an iterative manner. In particular, we first apply the exhaustive search algorithm to find the global optimal 2D position of the UAV. Subsequently, we can obtain the optimal UAV's flight altitude via monotonicity theory. Finally, by applying the Butler Matrix feed network, we propose a multi-beam generation scheme to optimize the beam patterns. Numerical results validate that the theoretical findings and demonstrate that significant performance gain in terms of energy harvesting of all ERs can be achieved by the proposed algorithm in UAV-assisted WPT networks.

1. Introduction

With the rapid development of Internet of Things (IoT), smart home, smart transportation system and smart city are widely used, resulting a large amount of data are generated from interconnected smart devices [1]. Meanwhile, the fifth generation (5G) mobile networks connect a large number of IoT devices will consume a significant amount of energy [2]. Therefore, extending the battery life of IoT devices plays a vital role in the development of 5G. Wireless power transfer (WPT) and energy harvesting (EH) are considered as the key technologies to extend battery life of devices [3]. In particular, There are two types of WPT technologies, namely, inductive coupling and magnetic resonance coupling. However, both of them have a short power transmission distance, and thus cannot support long-distance wireless charging. On the other hand, radio frequency (RF) energy transfer technology, radiated energy in the form of electromagnetic waves, has demonstrated to transfer energy over several kilometers [4].

In recent years, due to their autonomy, flexibility and mobility, unmanned aerial vehicles (UAVs) are widely deployed in various fields to offer cost-effective wireless services. Therefore, UAV-assisted WPT system has been proposed, where a UAV acts as an energy transmitter (ET) to charge a set of distributed energy receivers (ERs) on the ground. For example, in [5], the authors maximized the sum-energy transferred to ERs with the constraint of the maximum flight speed of the UAV. In [6], the author maximized the minimum uplink throughput by jointly optimizing the UAV flight trajectory and the transmission resource allocation in the UAV-assisted wireless powered communication networks, in which an UAV deployed as an ET can fly over a large area and charge multiple ERs distributed on the ground.

To further improve the energy transfer efficiency of the system, multi-antenna technology is used to effectively radiate RF signals to the desired ERs, which is also called energy beamforming. In particular, the antenna array is designed to realize high-gain main-lobe and reduce the side lobe to the minimum

* Corresponding author.
E-mail addresses: duan.xiangyang@zte.com.cn (X. Duan), 1472152862@qq.com (S. Ao), eewmfeng@mail.scut.edu.cn (W. Feng), eejtang@scut.edu.cn (J. Tang), hu.jc@nikolaimago.com (J. Hu).
[1] Senior Member, IEEE.

https://doi.org/10.1016/j.phycom.2020.101234
1874-4907/

required, and thus forms a sharp beam to greatly improve the energy transmission efficiency. For example, in [7], the author proposed two practical channel training methods, in which ET transmitted beamforming energy to a single antenna ER and receive energy feedback. In [8], an ET generated an energy beam to ERs and obtained energy measurement feedback in the multi-input multi-output (MIMO) system.

1.1. Main contributions

This paper studies the energy harvesting maximization problem in an UAV-assisted WPT network, in which the 3D position of the UAV and beam pattern are jointly optimized. In particular, we propose a multi-beam generation scheme based on the Butler Matrix feed network to further improve the energy transfer efficiency of the UAV. The contributions of this paper are as follows.

- This paper proposes a theoretical model for maximizing the energy harvested of all ERs in an UAV-assisted WPT network, where the 3D position of the UAV and beam pattern, flight altitude and wireless coverage performance of UAV are jointly taken into account. Due to the non-convexity of the energy acquisition optimization problem, we propose a low complexity iterative algorithm to optimize the 2D position and flight height of the UAV, and design the beam pattern with good performance.
- Firstly, given the fixed beam pattern, we use the exhaustive search algorithm to obtain the globally optimal 2D position of the UAV. Subsequently, the optimal flight altitude can be obtained via monotonicity theory. Finally, by applying the Butler Matrix feed network, we propose a multi-beam generation scheme to optimize the beam pattern in order to improve the wireless coverage of the UAV and serve multiple users.
- We provide numerical results to validate that the theoretical findings and demonstrate the performance gain in terms of energy harvesting of all ERs in UAV-assisted WPT networks.

1.2. Organization and notation

The following sections of this paper are organized as follows. In Section 2, the system model of the UAV-assisted WPT system is described, and the energy harvesting optimization problem based on the beam scanning principle is proposed. In Section 3, by applying the Butler Matrix feed network, we propose a low-complexity iterative algorithm to optimize the 3D position of the UAV and beam pattern. Section 4 gives the simulation results to verify the theoretical analysis, and finally the conclusion is given in Section 5.

2. System model and problem formulation

In this section, we first introduce the system model of the UAV-assisted WPT system and the principles of beam-scanning in antenna arrays, and then mathematically formulate the energy harvesting maximization problem.

2.1. System model

We consider a downlink WPT system which consisted of a rotary-wing UAV and K ERs randomly distributed on the ground. The UAV is equipped with N antennas while the ERs is equipped with single antenna. The UAV hovers above the ground and generates multi-beam to transmit RF signals to ERs, and the ERs are able to harvest energy from the received signals. After receiving the RF signals, the ER processes the signal in turn by the harmonic suppression filter, radio frequency rectifier and pass-through filter, and then transforms the signal into direct current (DC) energy which is managed by the energy manager, i.e. storing or supplying energy to ERs [9]. The architecture of the network is shown in Fig. 1.

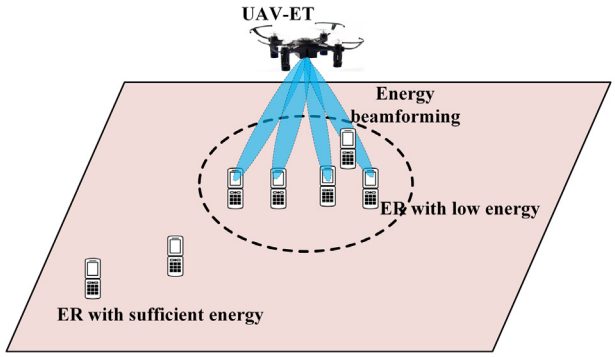

Fig. 1. Illustrations of an UAV-assisted WPT system with multi-beam.

Assuming that the location of ER $k \in \{1, 2, \ldots, K\}$ is represented by $z_k = (x_k, y_k)$. The location of the UAV is denoted by $z_u = (x_u, y_u)$ with altitude h. Since the wireless channel between the UAV and ER k is line-of-sight (LoS) dominated, the channel between the UAV and the ER k is given by [10]

$$\boldsymbol{h}_k = \sqrt{\beta_0 d_k^{-\alpha}}\boldsymbol{a}(\theta). \tag{1}$$

where β_0 denotes the channel power gain with reference $d_0 = 1m$, $\alpha(\alpha \geq 2)$ represents the path loss factor. $d_k = \sqrt{(x_k - x_u)^2 + (y_k - y_u)^2 + h^2}$ denotes the distance between the UAV and ER k. $\boldsymbol{a}(\theta)$ is a vector representing the phase difference from each antenna element to the ER k, i.e. the time difference between each antenna element and the ER k, which describes the angle between the beam direction and the normal direction of the array. Let N and d be the number of elements and the spacing between the elements, and λ be the wavelength. Consider a uniform linear array, $\boldsymbol{a}(\theta)$ can be expressed as

$$[\boldsymbol{a}(\theta)] = \left[1, \ldots, e^{j\frac{2\pi}{\lambda}nd\sin\theta}, \ldots, e^{j\frac{2\pi}{\lambda}(N-1)d\sin\theta}\right]^{\mathrm{T}}.$$

where $n \in \{0, 1, \ldots, N-1\}$ is the coordinate of the nth antenna elements. Therefore, the effective channel gain between the UAV and ER k is given by

$$|\boldsymbol{h}_k^H \boldsymbol{w}|^2 = \frac{\beta_0}{[(x_k - x_u)^2 + (y_k - y_u)^2 + h^2]^{\frac{\alpha}{2}}}|\boldsymbol{a}^H \boldsymbol{w}|^2. \tag{2}$$

From (2), $E(\theta) = \boldsymbol{a}^H(\theta)\boldsymbol{w}$ represents the synthesized pattern[2] of the array, where $\boldsymbol{w}$ is the beamforming vector that is used to offset the phase difference between antennas and to control the main beam directions, and will be further discussed later.

2.2. Beam scanning principle

For a linear array, the synthesized beam pattern can be expressed as [11]

$$E(\theta) = \sum_{n=0}^{N-1} p_n(\theta) I_n \times e^{jn(\frac{2\pi}{\lambda}d\sin\theta - \Delta\phi_m)}, \tag{3}$$

[2] The synthesized pattern is the distribution of the power density radiated by the antenna array stimulated in the far field. The pattern designed according to the specific scene can meet the basic needs of users.

where $p_n(\theta)$ and I_n are the element pattern[3] and amplitude excitation of the nth array element, respectively. $\Delta\phi_m$ is the progressive phase shift. The beamforming vector $\boldsymbol{w} = [w_0, \ldots, w_n, \ldots, w_{N-1}]^T$ describes the amplitude excitation and phase of each array element, $w_n = p_n(\theta)I_n \cdot e^{-jn\Delta\phi_m}$. For simplicity, we assume that the element pattern of the array is omnidirectional, and thus the influence of element patterns can be ignored. By omitting the element pattern, the synthesized beam pattern of the linear antenna array $E(\theta)$ is formulated as

$$F(\theta) = \sum_{n=0}^{N-1} I_n e^{jn(\frac{2\pi}{\lambda} d \sin\theta - \Delta\phi_m)}. \tag{4}$$

where $\Delta\phi = \frac{2\pi}{\lambda} d \sin\theta$ is termed the spatial phase difference, which describes the distance between antenna elements and the target. For uniformly distributed arrays, the spacing and excitation amplitudes of the array elements are the same. Therefore, I_n is normalized to 1 for all antenna elements, and (4) can be reformulated as

$$F(\theta) = \frac{1 - e^{jNX}}{1 - e^{jX}}. \tag{5}$$

where $X = \Delta\phi - \Delta\phi_m$. By applying Euler's formula,[4] (5) can be simplified as

$$F(\theta) = \frac{\sin\frac{N}{2}X}{\sin\frac{1}{2}X} e^{j\frac{N-1}{2}X}. \tag{6}$$

Since $\Delta\phi$ is very close to $\Delta\phi_m$ near the maximum of the main lobe, X is small enough and $\sin\frac{X}{2}$ is approximately equal to $X/2$, the far field intensity pattern of the linear array can be obtained as follows

$$|F(\theta)| = \frac{\sin\frac{N}{2}X}{\frac{N}{2}X} = \frac{\sin[\frac{N}{\lambda}\pi d(\sin\theta - \sin\theta_m)]}{\frac{N}{\lambda}\pi d(\sin\theta - \sin\theta_m)}. \tag{7}$$

$|F(\theta)|$ is the normalized antenna pattern with a maximum value of 1. When $|F(\theta)| = 1$, the beam direction θ_m of the antenna array can be obtained as follow

$$\sin\theta_m = \frac{\lambda}{2\pi d}\Delta\phi_m, \tag{8}$$

$$\theta_m = \arcsin(\frac{\lambda}{2\pi d}\Delta\phi_m). \tag{9}$$

The beam direction θ_m of the main lobe can be controlled by varying the phase difference $\Delta\phi_m$ which is provided by the phase shifters. Within the maximum scanning angle of the antenna array, the phase difference $\Delta\phi_m$ (i.e., the beamforming vector $w_n = p_n(\theta)I_n \cdot e^{-jn\Delta\phi_m}$) between the array elements is changed by the phase shifter, so that the generated beams are steered to the requesting users.

Another important indicator is the beamwidth of the antenna array, which refers to the width of the main lobe at $1/\sqrt{2}$ down value from the peak of the main beam. Therefore, when $|F(\theta)| = \frac{1}{\sqrt{2}}$, the beamwidth of the antenna array BW(in degrees) is given by

$$BW \approx 51\frac{\lambda}{Nd\cos\theta_m}. \tag{10}$$

By substituting the element spacing $d = \frac{\lambda}{2}$, (10) can be expressed as

$$BW \approx \frac{101}{N\cos\theta_m}. \tag{11}$$

It can be seen from (11) that the beamwidth of the antenna array is inversely proportional to $\cos\theta_m$; that is, the scanning angle θ_m increases with the increasing of beamwidth. (11) is valid for the case of large antenna arrays. As for small arrays, errors will inevitably occur in the results.

2.3. Energy harvesting optimization problem

We assume that the charging time $\tau_{k,\sigma}$ is fixed and the energy storage capacity of the ERs is large enough, so the energy harvested from RF signals by ER k is given by

$$\begin{aligned} Q_k &= \xi_k |\boldsymbol{h}_k^H \boldsymbol{w}|^2 P_0 \tau_{k,\sigma} \\ &= \frac{\xi_k \beta_0 P_0 \tau_{k,\sigma} |E(\theta)|^2}{[(x_k - x_u)^2 + (y_k - y_u)^2 + h^2]^{\frac{\alpha}{2}}}. \end{aligned} \tag{12}$$

where $\xi_k (0 < \xi_k < 1)$ represents the energy conversion efficiency due to the hardware circuits and energy conversion factors. P_0 is the transmit power of the UAV. From (12), the harvested energy of ER k is determined by the 3D placement of the UAV and beam pattern. Therefore, we aim to maximize the energy harvested of all ERs by optimizing the beam pattern and the 3D position of the UAV. Mathematically, this problem is formulated as

$$(P1): \max_{z_u, h, \boldsymbol{E}(\theta)} \sum_{k=1}^{K} \frac{\xi_k \beta_0 P_0 \tau_{k,\sigma} |E(\theta)|^2}{[\| z_k - z_u \|^2 + h^2]^{\frac{\alpha}{2}}}. \tag{13}$$

$$s.t. \quad \| z_k - z_u \|^2 \leq h^2 \tan^2\theta_m, \tag{14}$$

$$h_{\min} \leq h \leq h_{\max}. \tag{15}$$

By solving problem (P1), the optimal strategy $\{z_u^*, h^*, E^*(\theta)\}$ can be obtained. Constraint (14) guarantees that the largest horizontal distance between the UAV and ERs cannot exceed the coverage radius $h\tan\theta_m$. The converge radius of the UAV is related to the scanning angle θ_m and the hovering height h, where the UAV hovering altitude is restricted by the minimum altitude $h_{\min}$ and the maximum altitude $h_{\max}$ due to authority regulations [12]. The problem here, is mixed-combinatorial and non-convex and thus is difficult to solve. Therefore, we propose a joint 3D position optimization and multi-beam pattern design algorithm to optimize the UAV's 3D position and beam pattern, respectively.

3. Joint 3D position optimization and multi-beam design algorithm

3.1. Optimal UAV 2D location

To obtain the optimal 2D location of UAV, we fix the altitude h, beam pattern $E(\theta)$, and thus problem (P1) is reformulated as

$$(P2): \max_{x_u, y_u} \sum_{k=1}^{K} \frac{A_k}{[(x_k - x_u)^2 + (y_k - y_u)^2 + h^2]^{\alpha/2}}, \tag{16}$$

where $A_k = \xi_k \beta_0 P_0 \tau_{k,\sigma} |E(\theta)|^2$. However, problem (P2) is still non-convex, in this paper, we exploit the 2D exhaustive search to find the globally optimal solution (x_u^*, y_u^*) over the feasible region $[\underline{x}_u, \bar{x}_u]$ and $[\underline{y}_u, \bar{y}_u]$, where

$$\underline{x}_u = \min_{k\in K} x_k, \bar{x}_u = \max_{k\in K} x_k, \underline{y}_u = \min_{k\in K} y_k, \bar{y}_u = \max_{k\in K} y_k. \tag{17}$$

3.2. Optimal UAV altitude

Based on the solved 2D position of the UAV and the fixed beam pattern, we further obtain the optimal hovering altitude, and problem (P1) can be rewritten as

$$(P3): \max_{h} \sum_{k=1}^{K} \frac{A_k}{[D_k + h^2]^{\frac{\alpha}{2}}} \tag{18}$$

[3] The antenna element pattern refers to the radiation pattern when a single antenna is separately excited.

[4] The Euler's formula can be defined as $\sin x = \frac{e^{jx} - e^{-jx}}{2j}$ and $\cos x = \frac{e^{jx} + e^{-jx}}{2}$.

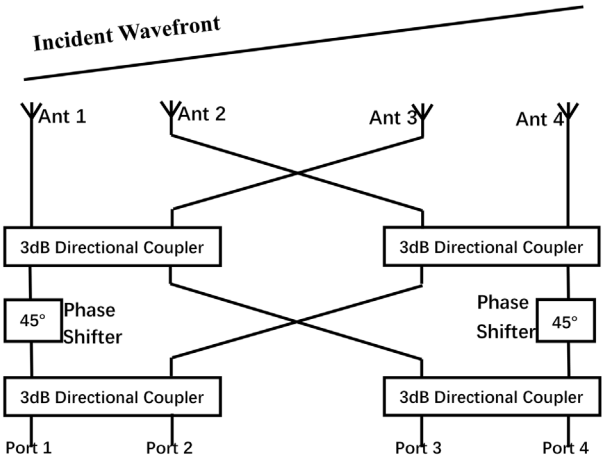

Fig. 2. Illustrations of a Butler Matrix feed network.

$$s.t.\ D_{\max} \le h^2 \tan^2 \theta_m, \tag{19}$$

$$h_{\min} \le h \le h_{\max}. \tag{20}$$

where $D_k = \| z_k - z_u \|^2$, $D_{max} = \max_{k=1}^{K} D_k$. From (18), it is shown that the hovering altitude h as the denominator is inversely proportional to the energy harvesting at the ERs. Therefore, the UAV's flight altitude should be as small as possible and is limited by the constrains (19) and (20), and therefore we can obtain the optimal hovering altitude as follows

$$h^* = \max\{\frac{\sqrt{D_{\max}}}{\tan\theta_m}, h_{\min}\}. \tag{21}$$

After obtaining the optimal 3D placement of the UAV, we then propose a multi-beam generation scheme to optimize the beam pattern by applying the Butler Matrix feed networks.

3.3. Optimal multi-beam pattern

As mentioned earlier, the direction of the main lobe is controlled by the phase difference between the array elements, and different scanning angles correspond to different phase differences. Therefore, different sets of phase differences are provided to the antenna array, which can generate multiple separated radiation beams. Based on this principle, a Butler Matrix feed network is designed, which provides different phase differences at output ports to radiate multiple beams. As shown in Fig. 2, the basic components of the Butler Matrix feed network are 3 dB directional couplers and fixed phase shifters [13]. In addition, we use cross-couplers to avoid overlap of the microstrip lines in the circuits and reduce the influence on the performance of the circuits.

3.3.1. 3 dB directional coupler

The 3 dB directional coupler is also known as branch line coupler, and its structure is shown in Fig. 3. The principle is that the excitation energy from port P1 is divided equally to ports P2 and P3, and the phase difference between two ports is 90 degrees. The remaining port P4 is called the isolated end; that is, no energy is coupled to this port. The branch-line hybrid network is highly symmetric, and all four ports can be used as the input ports. The two output ports are always on the other side of the network, while the isolated port is located on the same side as the input ports [14].

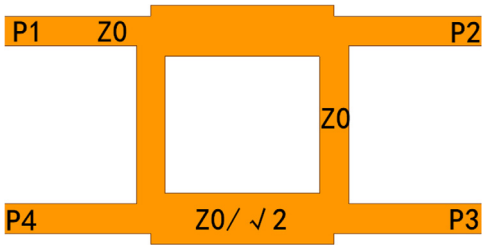

Fig. 3. The architecture of branch line coupler in electromagnetic simulation software HFSS.

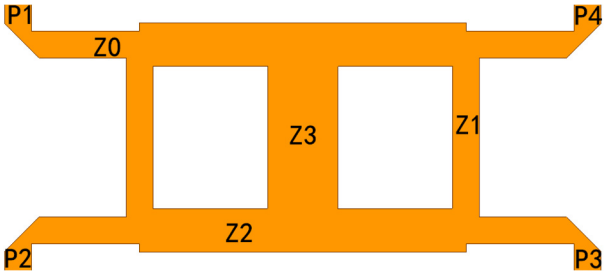

Fig. 4. The architecture of two-section branch line coupler in electromagnetic simulation software HFSS.

3.3.2. Cross-coupler

The intersection of transmission lines is inevitable in the design of microwave circuits. The most common solutions are the use of air-bridges and under-passes. In [15], the author proposed an improved scheme for the branch-line coupler design, which solved the problem of transmission lines crossing and provided the return loss[5] and isolation[6] better than 20 dB, as well as widened the effective working bandwidth. Such a component used to solve the problem of line crossing in Butler Matrix feed network is called cross-coupler. In this paper, the two-section branch-line structure in [15] is applied to improve the performance of the Butler Matrix feed networks.

As shown in Fig. 4, the two-section branch-line coupler theoretically couples the excitation signal lossless from port P1 to port P3, and ports P2 and P4 are isolated ends. Similar to the 3 dB directional coupler, the two-section branch line coupler is also highly symmetrical. All ports can be used as the input port and the output port on its diagonal side is to avoid crossover of the transmission line. According to [15], the specific parameters[7] of the two couplers are: $Z_0 = 50\ \Omega, Z_1 = \frac{Z_0^2}{50}, Z_2 = \frac{Z_0}{\sqrt{2}}, Z_3 = \frac{50Z_2^2}{Z_0^2}$.

The $N \times N$ Butler Matrix means that the Butler feed network has N input ports and N output ports, which is an analog implementation of Fast Fourier Transform (FFT). In particular, the excitation signal is fed from the input ports (i.e., the feed network of the antenna array), and a set of progressive phases is generated at the output ports. The set of progressive phases can compensate the spatial phase difference between the antenna array and the ERs, and thereby control the radiation pattern and gain of the antenna array. N different ports can have N different sets of progressive phases. This means that N beams can be formed to serve multiple ERs. In addition, given the fact that the components and

[5] Return loss is a parameter that indicates the reflective performance of a component, meaning that a portion of the incident power is reflected back to the source.

[6] Isolation is a measure of the ability to isolate forward and backward waves.

[7] Z corresponds to the impedance of the microstrip line, which affects the characteristics of the microstrip circuit.

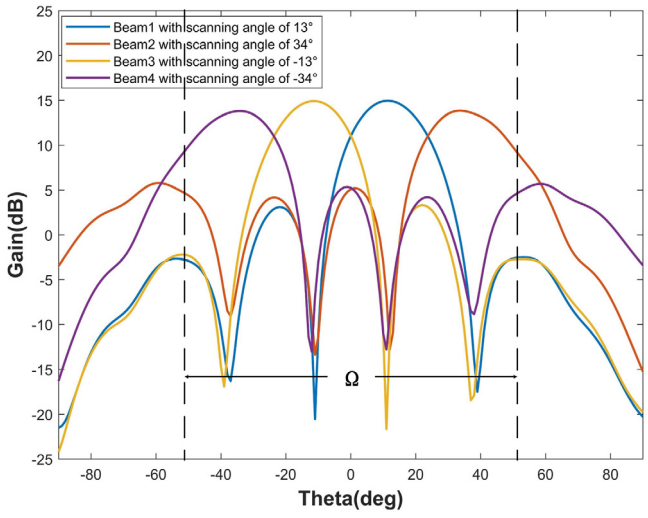

Fig. 5. Sector area covered by multiple beams in planar graphics.

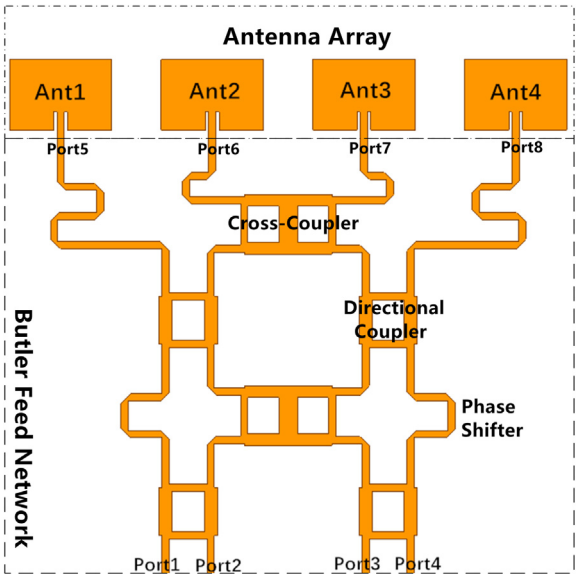

Fig. 6. Actual design diagram of multi-beam antenna array in electromagnetic simulation software HFSS.

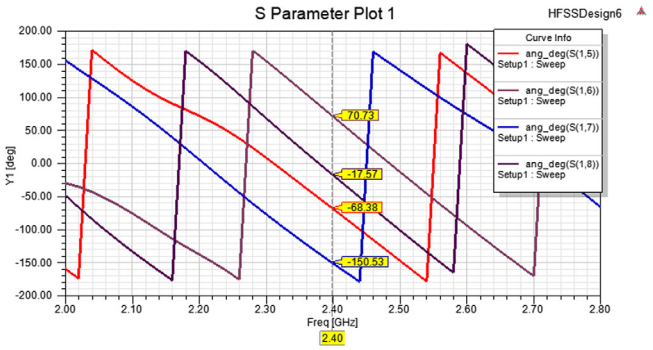

Fig. 7. Phases of the four output ports when Port1 is excited (operating frequency is 2.4G).

the overall layout of the feed network are symmetric, all of the generated beams are also highly symmetrical. Thus, N must be an integer exponential of 2.

According to [11,13], the normalized far field pattern of the pth beam is given by

$$|F_p| = \frac{\sin\frac{N}{2}(\frac{2\pi}{\lambda}d\sin\theta - \frac{2p-1}{N}\pi)}{N\sin\frac{1}{2}(\frac{2\pi}{\lambda}d\sin\theta - \frac{2p-1}{N}\pi)}. \tag{22}$$

where N is the number of array elements. Thus, similar to (8) and (10), the direction of the pth beam is given by

$$\sin\theta_p = \frac{2p-1}{2Nd}\lambda. \tag{23}$$

The beamwidth of the antenna array is expressed as

$$BW \approx 51\frac{\lambda}{Nd\cos\theta_p}. \tag{24}$$

From (23) and (24), the spatial range Ω covered by the multi-beam Butler Matrix feed network can be obtained. For a linear array of $N = 2^k$ (k is a constant) units, N beams can be formed, and they can form $N/2$ beams on both sides of the array normal. Therefore, the coverage range of N beams should be

$$\Omega = 2\theta_p + BW. \tag{25}$$

Using the above principle, we designed and simulated a 4×4 Butler Matrix through the electromagnetic simulation software HFSS, including four 3 dB directional couplers, two cross-couplers, and two fixed phase shifters. The designed Butler Matrix feeds excitations with equal amplitude and phase difference into a 1×4 antenna array to generate four steering beams.

4. Simulation results

In this section, simulations results are provided in order to validate the performance of the proposed joint 3D position optimization and multi-beam design algorithm. Because 2.4G signals are has longer transmission distance and lower signal loss when propagating in air or obstacles, and most devices currently use 2.4G band, the system is designed to operate at 2.4G for universality.

4.1. Multi-beam antenna array

In the light of the theory mentioned above, a 4×4 Butler Matrix feed network operating at 2.4 GHz is designed and simulated for demonstrating the performance of the multi-beam generation scheme. The output ports provide four sets of phase differences (i.e., $\pm45°$ and $\pm135°$) for the antenna array, where the antenna array corresponds to a 4-element linear array. According to (23) and (25), the elevation angles of the desired four beams are $\pm14.5°$ and $\pm48.6°$, respectively, and the maximum angular coverage Ω is $-61.2° \sim +61.2°$. Fig. 6 shows a multi-beam array designed and simulated by the electromagnetic simulation software, i.e, HFSS, which is composed of a 4×4 Butler Matrix feed network and a 1×4 linear array.

4.1.1. 4×4 Butler matrix

Fig. 7 shows the performance of our proposed Butler Matrix feed network. When port1 is excited, four output ports can generate the phases. As shown in Fig. 7, the phase difference between Port5 and Port6 is 139.11°, the phase difference between Port6 and Port7 is 138.74°, and the phase difference between Port7 and Port8 is 132.96°. Compared with the theoretical value of 135°, the maximum error is 4.11°, which is caused by the parasitic coupling phenomenon in the circuit.

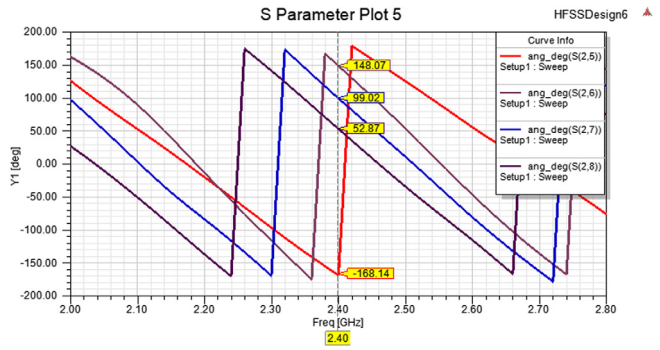

Fig. 8. Phases of the four output ports when Port2 is excited (operating frequency is 2.4G).

Similarly, when port2 is excited, the theoretical value of the phase difference between adjacent ports is $-45°$. As shown in Fig. 8, it is shown that the phase difference between port5 and port6 is $-43.79°$, the phase difference between port6 and port7 is $-49.05°$, and the phase difference between port7 and port8 is $-46.15°$. Compared with the theoretical value, the maximum error is 4.05°.

In addition, due to the symmetry of Butler Matrix feed network, when input port3 is excited, the phase difference between adjacent ports is 45°; when input port4 is excited, the difference between adjacent ports is $-135°$. The maximum errors are both less than 5°. From the analyses of the simulation results, the measured values of our proposed Butler Matrix feed network is close to the theoretical values.

4.1.2. Antenna array

The antenna array is composed of 4 microstrip antennas that operates at 2.4 GHz. The role of the antenna is to convert the guided waves into electromagnetic waves in free space, but the power radiated by a single antenna is omnidirectional, low gain and low efficiency, as shown in Fig. 9. Therefore, the large-scale antenna array and beamforming technology are used to concentrate the radiated energy into a narrow beam and steer to a specified user, thereby significantly increasing the energy efficiency of ERs.

Fig. 10 shows the radiation pattern of the multi-beam antenna array. The signals pass through the Bulter Matrix feed network and radiate to the ERs through an antenna array. When port1 is excited, the Butler Matrix feed network provides signals with a 135° phase difference to the antenna array, and the beam direction is 34° away from the normal direction of the antenna array, as shown in Fig. 10(a). When port2 is excited, the Butler Matrix feed network gives the signals with a $-45°$ phase difference to the antenna array, and main-lobe direction is $-13°$ away from the normal direction of the antenna array, as shown in Fig. 10(b). Due to the symmetry of Butler Matrix feed network, when port3 and port4 are excited, the scanning angle is 13° and $-34°$, respectively, as shown in Fig. 10(c) and (d). In addition, it can be seen from Fig. 10 that the gain of the four beams is greater than 13.8 dB. Thus, the simulation results demonstrate that our proposed network has a high directivity and radiation gain in the main-lobe directions.

4.2. Multi-beam UAV system

Figs. 11–12 show the energy harvesting performance of ERs. We assume that the UAV has a minimum hovering altitude of 21 m and a maximum of 120 m [16]. The transmit power of the UAV P_0 is 10 W, the charging time $\tau_{k,\sigma}$ for ER k is 5 s, the path

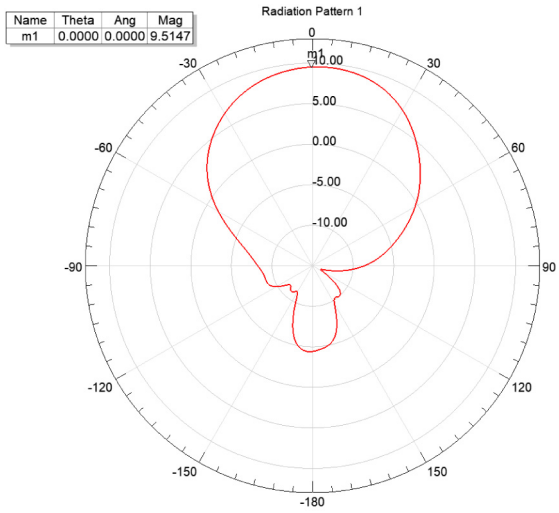

(a) Radiation pattern

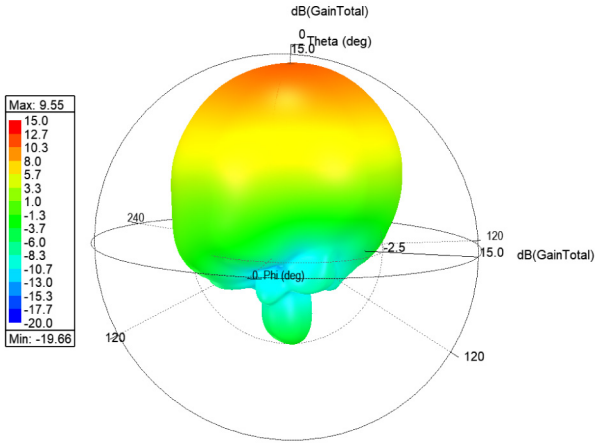

(b) 3D polar plot

Fig. 9. Simulation results of a 2.4 GHz Microstrip Patch Antenna.

loss factor α is 2, and the conversion efficiency ξ_k of ER k is set to 0.5 [17]. As shown in Fig. 5, the scanning range of the antenna array is determined by the four beams together, and the desired coverage range Ω is $-47.86° \sim +47.70°$. It is assumed that $K = 11$ ERs are randomly distributed over a range of 500×500 m^2. As shown in Fig. 11, the serving area can be roughly divided into four regions, which are respectively composed of ER 1–2, ER 3 –4, ER 5 – 8 and ER 9 – 11. Then, from (21), we can calculate the optimal hovering flight h^* at each waypoint, which are 43.7 m, 38.1 m, 76.1 m and 74.7 m respectively. It is observed in Fig. 11 that the UAV is located in the middle of all ERs in order to maximize the sum harvested energy of all ERs.

Fig. 12 shows the received power of each ER. As shown in Fig. 12, the ERs that are closer to the UAV can receive more energy than the far ERs, such as ER 6, ER 11. The collected energy as shown in Fig. 12 is approximately 1.68 W at the minimum and 3.37 W at the maximum. This implies that the optimal 3D locations of the UAV can improve the received power of ERs. Therefore, it is demonstrated that our proposed joint 3D position optimization and multi-beam design algorithm can significantly improve the system performance in terms of sum harvested energy of all ERs.

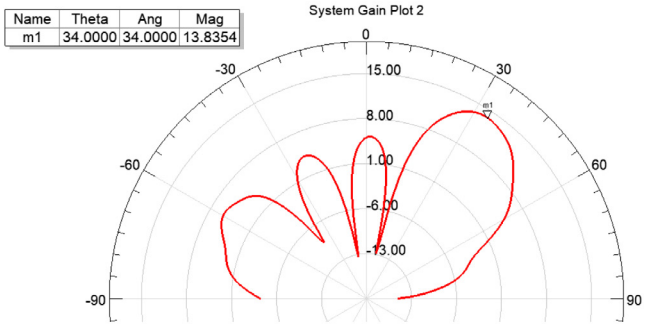

(a) Port1 is excited.

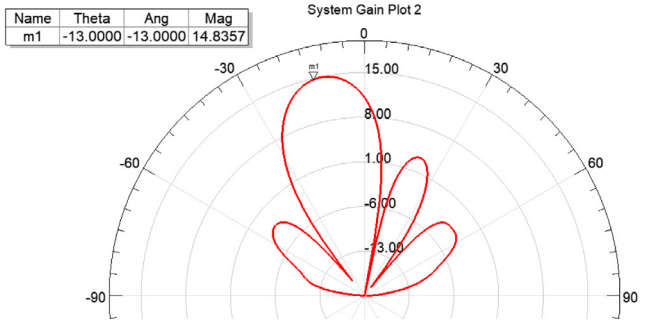

(b) Port2 is excited.

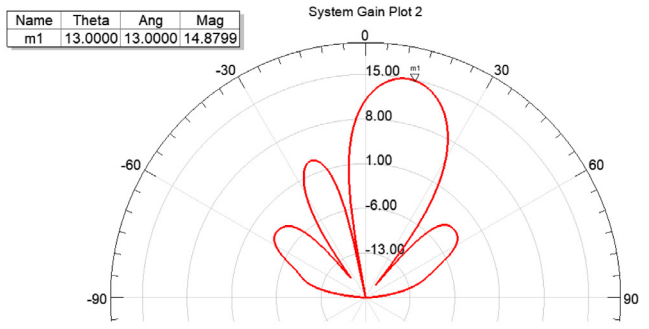

(c) Port3 is excited.

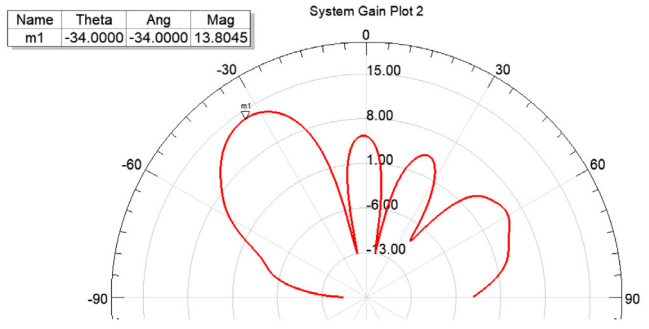

(d) Port4 is excited.

Fig. 10. Radiation pattern of the multi-beam antenna array.

5. Conclusion

In this paper, we study the harvested energy maximization problem in UAV-enabled WPT systems, where the UAV acts as a wireless charger and transmits energy to a group of users. In particular, the UAV equipped with a linear antenna array fed by a Butler Matrix feed network generates multi-beam to serve multiple ERs. We aim to maximize the total harvested energy at all ERs via optimizing the 3D position of the UAV and the beam pattern. Due to the intractability and non-convexity of this optimization problem, we propose a joint 3D position optimization and multi-beam design algorithm to decompose the considered problem into three sub-problems and solve them sequentially. Specifically, the 2D exhaustive search method is adopted to optimize the horizontal locations of the UAV. Then, the flight altitude is obtained directly by monotonicity theory. Finally, we propose a multi-beam generation scheme based on the Butler Matrix feed network to optimize the beam pattern. Numerical results illustrate that the energy harvesting performance of all ERs can be significantly improved by the proposed algorithm.

However, the algorithm does not take the flight trajectory of the UAV into account. In the subsequent research, we will further consider the requests of users in a certain area at the same time period, and design an optimal flight trajectory to further reduce the energy consumption of the UAV.

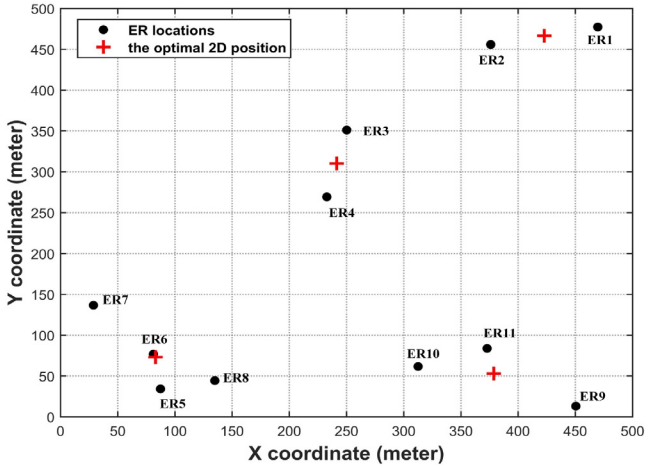

Fig. 11. Optimal 2D locations in an UAV-assisted WPT system with K = 11 ERs.

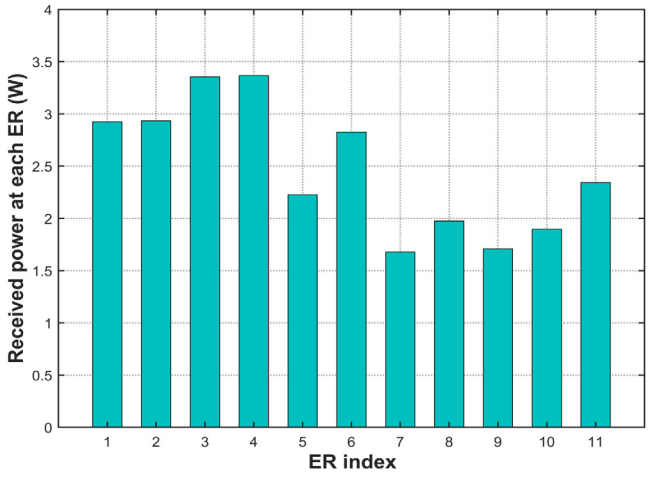

Fig. 12. Energy harvesting by each energy receiver.

Declaration of competing interest

The authors declare that they have no known competing financial interests or personal relationships that could have appeared to influence the work reported in this paper.

References

[1] G.A. Akpakwu, B.J. Silva, G.P. Hancke, A.M. Abu-Mahfouz, A survey on 5G networks for the internet of things: Communication technologies and challenges, IEEE Access 6 (2018) 3619–3647.

[2] J. Wang, L. Zhao, J. Liu, N. Kato, Smart resource allocation for mobile edge computing: A deep reinforcement learning approach, IEEE Trans. Emerg. Top. Comput. (2020) in press.

[3] L. Zhao, J. Wang, J. Liu, N. Kato, Routing for crowd management in smart cities: A deep reinforcement learning perspective, IEEE Commun. Mag. 57 (4) (2019) 88–93.

[4] Q. Luo, Y. Cao, J. Liu, A. Bensilmane, Localization and navigation in autonomous driving: Threats and countermeasures, IEEE Wirel. Commun. (2020) in press.

[5] J. Wang, J. Liu, N. Kato, Networking and communications in autonomous driving: A survey, IEEE Commun. Surv. Tutor. 21 (2) (2018) 1243–1274.

[6] S. Li, L.D. Xu, S. Zhao, 5G internet of things: A survey, J. Ind. Inf. Integr. 10 (2018) 1–9.

[7] Egham, Gartner says 8.4 billion connected "Things" will be in use in 2017, up 31 percent from 2016, [Online]. Available: https://www.gartner.com/newsroom/id/3598917.

[8] J. Tang, D.K.C. So, N. Zhao, A. Shojaeifard, K.-K. Wong, Energy efficiency optimization with SWIPT in MIMO broadcast channels for internet of things, IEEE Internet Things J. 5 (4) (2018) 2605–2619.

[9] J. Tang, D.K.C. So, A. Shojaeifard, K.-K. Wong, J. Wen, Joint antenna selection and spatial switching for energy efficient MIMO SWIPT system, IEEE Trans. Wirel. Commun. 16 (7) (2017) 4754–4769.

[10] W. Feng, N. Zhao, S. Ao, J. Tang, X. Zhang, Y. Fu, D.K.C. So, K.K. Wong, Joint 3D trajectory design and time allocation for UAV-enabled wireless power transfer networks, IEEE Trans. Veh. Technol. 69 (9) (2020) 9265–9278.

[11] Y. Sun, D. Xu, D.W.K. Ng, L. Dai, R. Schober, Optimal 3D-trajectory design and resource allocation for solar-powered UAV communication systems, IEEE Trans. Commun. 67 (6) (2019) 4281–4298.

[12] Y. Zeng, R. Zhang, Energy-efficient UAV communication with trajectory optimization, IEEE Trans. Wirel. Commun. 16 (6) (2017) 3747–3760.

[13] C. Zhan, Y. Zeng, R. Zhang, Trajectory design for distributed estimation in UAV-enabled wireless sensor network, IEEE Trans. Veh. Technol. 67 (10) (2018) 10155–10159.

[14] H. Wang, G. Ren, J. Chen, G. Ding, Y. Yang, Unmanned aerial vehicle-aided communications: Joint transmit power and trajectory optimization, IEEE Wirel. Commun. Lett. 7 (4) (2018) 522–525.

[15] J. Xu, Y. Zeng, R. Zhang, UAV-enabled wireless power transfer: Trajectory design and energy optimization, IEEE Trans. Wirel. Commun. 17 (8) (2018) 5092–5106.

[16] L. Xie, J. Xu, R. Zhang, Throughput maximization for UAV-enabled wireless powered communication networks, IEEE Internet Things J. 6 (2) (2019) 1690–1703.

[17] M. Alzenad, A. El-Keyi, F. Lagum, H. Yanikomeroglu, 3-D placement of an unmanned aerial vehicle base station (UAV-BS) for energy-efficient maximal coverage, IEEE Wirel. Commun. Lett. 6 (4) (2017) 434–437.

Xiangyang Duan received his B.E. and M.E. degrees in mechanical engineering and material processing engineering from Tsinghua University, Beijing, China, in 1999. He works at ZTE Corporation, Shenzhen, China, where he researches the universal mobile telecommunications system, baseband units, and wireless system architecture. His research interests include 5G technology and mobile edge computing as well as novel services and applications for future mobile networks.

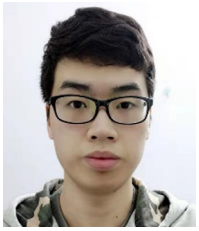

Shaopeng Ao received his B. Eng. degree in the school of Physics and Electronics at the Henan University, Henan, China, in 2017. He is currently pursuing his M.Sc. at the School of Electronic and Information Engineering, South China University of Technology, China, under the supervision of Prof. Jie Tang. His research interests include Antenna design and optimization, Wide angle scanning of antenna array, Multi-beam optimization and 5G networks.

Wanmei Feng received her M.Sc. degree (with Distinction) in the Department of Physics and Telecommunications Engineering at the South China Normal University (SCNU), Guangzhou, China, in 2018. She is currently pursuing her Ph.D degree at the School of Electronic and Information Engineering, South China University of Technology, China, under the supervision of Prof. Jie Tang and Prof. Yuli Fu. Her research interests include energy efficiency optimization, UAV communications, non-orthogonal multiple access, simultaneous wireless information and power transfer and 5G network.

Jie Tang (S'10–M'13-SM'18) received the B.Eng. degree in Information Engineering from the South China University of Technology, Guangzhou, China, in 2008, the M.Sc. degree (with Distinction) in Communication Systems and Signal Processing from the University of Bristol, UK, in 2009, and the Ph.D. degree from Loughborough University, Leicestershire, UK, in 2012. From 2003 to 2015, he was a research associate at the School of Electrical and Electronic Engineering, University of Manchester, UK. He is currently a full professor at the School of Electronic and Information Engineering, South China University of Technology, China.

His current research centers around 5G and beyond mobile communications, including topics such as massive MIMO, full-duplex communications, edge caching and fog networking, physical layer security, wireless power transfer and mobile computing. He is a senior member of IEEE, CIE and CIC, and currently serving as an Editor for IEEE Wireless Communications Letters, IEEE Access, and EURASIP Journal on Wireless Communications and Networking. He also served as a track cochair for IEEE VTC-Spring 2018, EAI GreeNets 2019, ICCC Workshop 2019 and ICCC 2020. He is a co-recipient of the 2018 IEEE ICNC, 2018 CSPS and 2019 IEEE WCSP Best Paper Award.

Juncheng Hu received the B.Eng. degree in Telecommunications Engineering from the Hunan University of Science and Technology, Hunan, China, in 2007, the M.Sc. degree in Mobile Communications Engineering from Loughborough University, Leicestershire, UK, in 2008, and the Ph.D. degree from Loughborough University, Leicestershire, UK, in 2013. From 2014 to 2017, he was a System Integration Engineer at CSE Transtel Pte Ltd, SG. He is currently a Senior Lecturer at the School of Humanity and Management, Guilin Medical University, China.

His current research centers around the application of big data of medical information and artificial intelligence of medical image in early screening for gastric cancer and myocardial infarction.